Research on Optimum Heating System Design for Rapid Thermal Response Mold with Electric Heating Based on Response Surface Methodology and Particle Swarm Optimization

Guilong Wang,[1,2] Guoqun Zhao,[1,2] Yanjin Guan[1,2]

[1]*Key Laboratory for Liquid-Solid Structural Evolution and Processing of Materials (Ministry of Education), Department of Materials Science & Engineering, Shandong University, Jinan, Shandong 250061, People's Republic of China*
[2]*Engineering Research Center for Mold & Die Technologies, Department of Materials Science & Engineering, Shandong University, Jinan, Shandong 250061, People's Republic of China*

Received 24 January 2010; accepted 12 May 2010
DOI 10.1002/app.32771
Published online 29 July 2010 in Wiley Online Library (wileyonlinelibrary.com).

ABSTRACT: A new electric-heating rapid thermal response (RTR) mold with floating cavity/core for rapid heat cycle molding is investigated in this study. Process principles of Rapid heat cycle molding (RHCM) with such new electric-heating mold are discussed and presented. Response surface methodology (RSM) is employed to develop mathematical relationships between layout of the heating elements and heating efficiency, temperature uniformity and structural strength of the floating cavity. Three explanatory variables including half distance between two adjacent heating rods, spacing between heating rods and cavity surface, and the diameter of the heating rod are used to describe the layout and scale of the heating elements. The response variables involving required heating time, maximum cavity surface temperature, and maximum von-Mises stress are used to characterize heating efficiency, temperature uniformity, and structural strength of the floating cavity, respectively. Central composite design (CCD) method is used for factorial experiments. Finite element analyses are conducted for combination of explanatory parameters to acquire the corresponding values of the response variables. Three predictive models for the response variables are created by regression analysis. Analysis of variance (ANOVA) is used to check their accuracy. These response surface models are interfaced with an effective particle swarm algorithm for the optimum heating system design of the electric-heating RTR mold. The developed optimum method is then used for the design of the floating electric-heating cavity for an actual industrial product. The following heat transfer analysis results show that the temperature distribution uniformity of the cavity surface is greatly improved with the optimal cavity structure and layout of heating rods. © 2010 Wiley Periodicals, Inc. J Appl Polym Sci 119: 902–921, 2011

Key words: rapid heat cycle molding; RHCM; rapid thermal response mold; electric heating; response surface methodology; particle swarm optimization; multi-objective constraint optimization

INTRODUCTION

Due to the rapid development of the 3C (Computer, Communication, and Consumer electronic) industries, plastic parts are demanded to become much lighter, thinner, and also with high appearance and accuracy. It is becoming more and more difficult for conventional injection molding to satisfy such requirements for plastic parts. To solve this problem, a new injection molding process, called rapid heat cycle molding (RHCM), has been paid more and more attention and is becoming more widely used in recent years. This new molding process can achieve rapid mold temperature variation by rapid heating and cooling techniques. Due to the extremely high mold temperature in RHCM, polymer melt can fill mold cavity easily and replicate cavity geometry precisely. In addition, the elevated high mold temperature can also prevent the solidification of the melt and promote integration of different melt interfaces. As a result, surface defects, such as welding mark, flowing mark, jetting, etc., usually occurring in conventional injection molding can be greatly alleviated or even completely eliminated.

Correspondence to: G. Zhao (zhaogq@sdu.edu.cn).
Contract grant sponsor: National Science & Technology Pillar Program in the Eleventh Five-year Plan Period of the People's Republic of China; contract grant number: 2006BAF02A05.
Contract grant sponsor: Shandong Province High Technology Innovation Engineering Special Plan Program; contract grant number: 2008ZZ10.
Contract grant sponsor: Program for New Century Excellent Talents in University; contract grant number: NCET-08-0337.

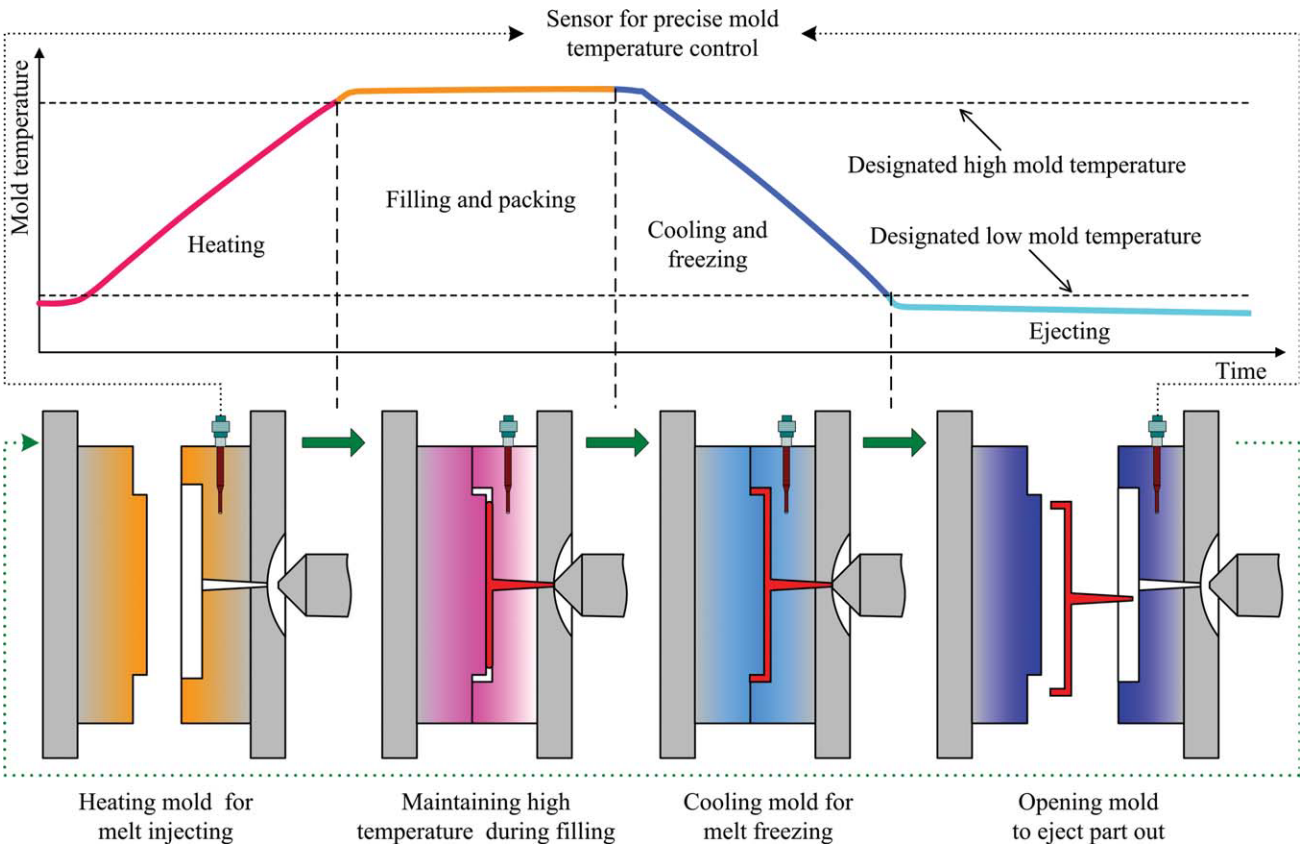

Figure 1 Process principle and mold temperature variation of RHCM. [Color figure can be viewed in the online issue, which is available at wileyonlinelibrary.com.]

Therefore, perfect part surfaces can be achieved in RHCM. The pollutive secondary operations such as sanding and painting to improve surface appearance of plastic parts produced with conventional injection molding are not needed any more. Therefore, the entire production process can be shortened. As filling process proceeds when mold cavity surface temperature is high enough in RHCM, filling pressure can be evenly transmitted to the end of the mold cavity and a much more balanced filling pressure distribution can be obtained. Thus, residual stress, warpage, and distortion of the part can be reduced. Due to the above mentioned characteristics and advantages, RHCM process is much more suitable to produce super glossy, paintless, extreme thin-wall, and optical parts, or the products with microstructures, such as, LCD TV frames,[1–2] optic lens,[3] light-guided plates,[4] and micro gears.[5]

Similar to conventional pulsed cooling method in injection molding process,[6–8] the aim of mold temperature control in RHCM is also to achieve a rapid, variable, and accurate cavity surface temperature control. By doing this, the part quality, especially surface appearance, can be improved with little effect on molding cycle time. However, the mold in RHCM process should not only be rapidly cooled after melt filling but also be rapidly heated to a high temperature by some special heating technique right before melt injection to prevent premature cooling of the melt and facilitate melt filling. According to mold temperature variation in RHCM process, the whole molding cycle can be divided into four different stages. In the first stage, the mold is rapidly heated to a designated high temperature, usually higher than the glass transition temperature or melt temperature of the polymer material, before filling process. At the same time, polymer pellets are transferred into molten state by heating and shearing for preparation of melt injecting. In the following stage, the molten polymer is injected out to fill mold cavity. After filling, extra molten material should be delivered into the mold cavity by high injection pressure to compensate for the shrinkage and ensure complete filling. In the third stage, the mold is cooled rapidly to solidify the shaped polymer melt in mold cavity for part injection. In the final stage, the mold is opened to eject out the plastic part right after the cooling process is finished. Figure 1 shows the process principle and mold temperature variation of RHCM.

For mass production of RHCM, rapid mold temperature variations are very necessary to shorten molding cycle time and achieve an economical productivity. Therefore, special heat/cool techniques and mold structure for rapid thermal response

should be developed for RHCM. The main factors affecting thermal response of the mold include the following factors: heating technique, cooling technique, and mold structure. In the past several years, a lot of heating methods and heating devices have been developed and constructed to achieve rapid mold heating for RHCM. These heating methods include resistance heating,[2,9–11] induction heating,[4,5,12,13] infrared heating,[14,15] and convection heating with hot fluids.[1,16,17] For rapid mold cooling after filling and packing, the conventional cooling method used in conventional injection molding process by circulating cold water in the mold channels can be utilized in RHCM. However, the coolant temperature should be lowered and the coolant flow speed should be increased enough to achieve a reasonable cooling efficiency. From the view of mold design and construction, it is best to minimize the amount of mold material to be thermally cycled in RHCM to decrease the thermal mass of the mold. In addition, a good insulation for the mold steel is also very useful to improve heating and cooling efficiencies. Based on these objectives, some novel mold structures have been proposed, such as multilayer mold[9,18,19] and scaffolded mold.[5,20–22] In this study, a new electric-heating RTR mold with floating cavity/core is investigated. Factorial experiments based on central composite design method are conducted by finite element analysis to study the effect of the layout of heating elements on thermal response efficiency, temperature uniformity, and structural strength of the floating cavity. An efficient multiobjectives optimization method by integrating response surface methodology and particle swarm algorithm is developed to optimize the layout of the heating elements in the floating cavity of electric-heating RTR mold.

ELECTRIC-HEATING RTR MOLD WITH FLOATING CAVITY/CORE

As a common heating technique, electric heating has been used in injection molding industry for many years. However, because of its low heating efficiency and large energy consumption, it is usually used for local mold heating in conventional injection molding. Further, the following long cooling time after filling for convention mold also restricts its application. By contrasting with those surface heating methods, such as induction heating and infrared heating, it seems like that interior heating method of electric heating is not a good choice for rapid mold heating in RHCM although it is much more robust, stable, and economical. However, if we can greatly decrease the thermal mass of the mold that should be thermally cycled in injection molding process, it will be possible to apply this mature heating technique for whole mold heating in RHCM. For instance, the multilayer RTR mold designed by Yao et al.[9] can be heated from 25 to 250°C in 2 s and then cooled to 50°C in 10 s. Such high heating efficiency is because that only a thin and high conductive heating layer coated as the cavity surface is heated and the thermal mass of the RTR mold is very low. But the short lifetime of the multilayer mold due to the low bonding strength between different layers restricts its application in mass production. To reduce the thermal mass of the mold cavity/core, the authors design a new electric-heating RTR mold with floating cavity/core.[23] Heating rods or pipes buried in the cavity/core are used to raise cavity surface temperature and cooling water circulating in separate cooling plates is used to cool the cavity/core. The following sections will expound the electric-heating RTR mold with a floating cavity and heat transfer in it.

Mold structure and work principle

Figure 2 shows the typical structure of the electric-heating RTR mold with a floating cavity and core. As it can be seen from Figure 2(a), when the mold is in the open state, the cavity and core can move forward by the elastic force of the springs to separate with the corresponding cooling plates. During mold opening, the cavity and core will be heated by the heating rods buried in them after the plastic part is fully ejected out. Contrasting with conventional injection mold, thermal mass of the cavity, and core in the new electric-heating RTR mold is much smaller owing to their thinner thickness in cavity surface regions. Further, the air gaps between the floating cavity/core and the corresponding cooing plates are good insulation layers and can greatly reduce heat loss. Therefore, the floating cavity and core can be heated rapidly with low thermal consumptions. When cavity and core are heated to the designated high temperature, mold heating is stopped by cutting off the power of the heating rods. Then, the mold starts to be closed for mold filling process. During mold closing process, the floating cavity and core will be pressed to move back forward gradually by the clamping force until they completely contact with the cooling plates. After the mold is completely closed as shown in Figure 2(b), molten polymer is injected into mold cavity. In the following filling process, the elevated high cavity surface temperature can ensure superior flowability and transferability of the polymer melt. In addition, cooling process starts as soon as the floating cavity and core contacts the cooling plates, in the cooling channels of which cooling water is circulated. Generally, the delay time for the cavity surface temperature to reduce due to cooling can ensure a complete

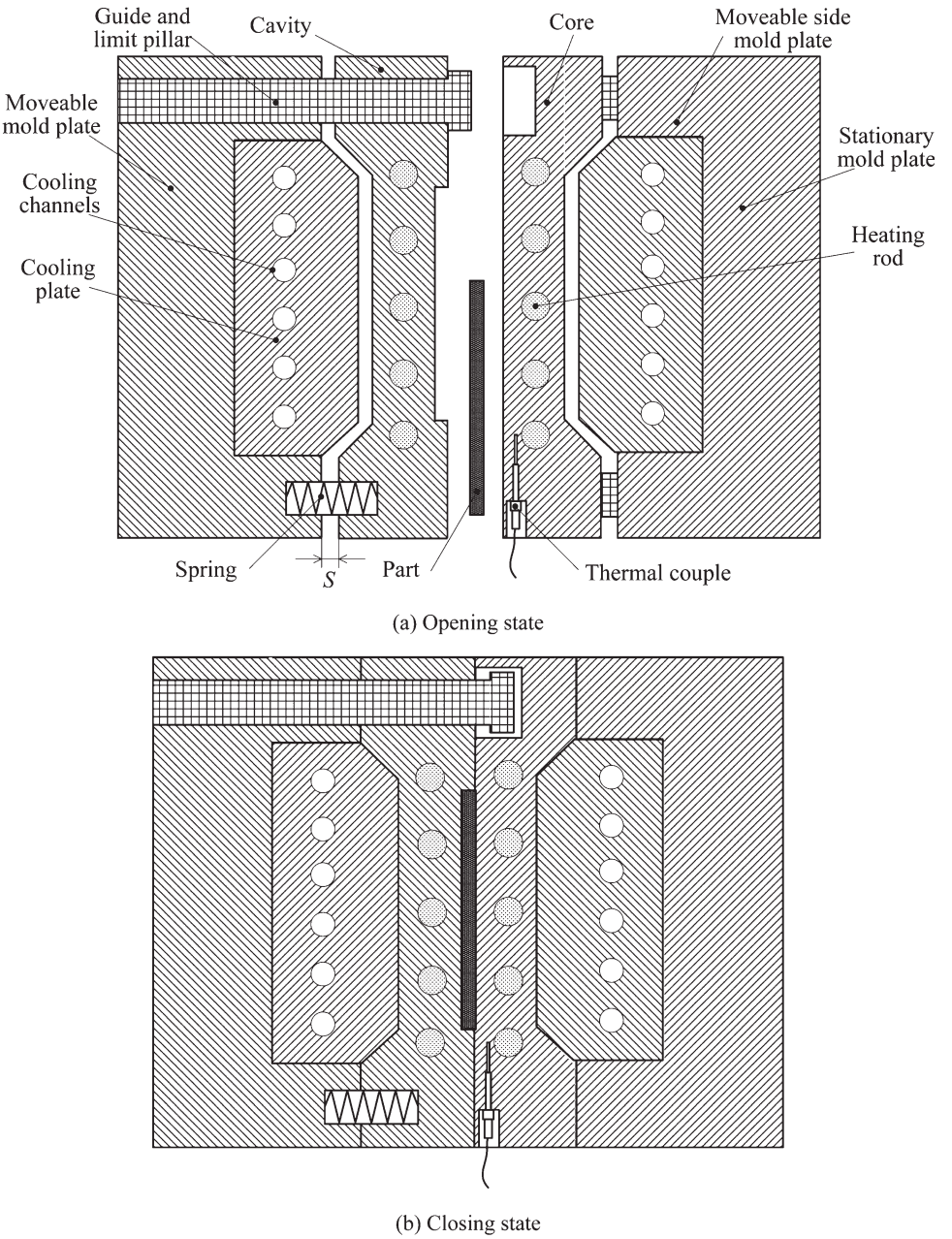

Figure 2 The typical structure of an electric heating RTR mold with floating cavity and core: (a). opening state, (b) closing state.

filling of the mold cavity. The materials with good heat transfer ability, such as aluminum and copper, or their alloys can be chosen as the materials of the cooling plates to improve cooling efficiency. Therefore, the cooling time can be reduced to achieve a short molding cycle time of RHCM. During the forward and backward movements of the floating cavity and core, guide and limit pillars as shown in Figure 2(a) can not only ensure their motion directions, but also limit their movement distances (S) for accurate reposition to ensure complete contact with the cooling plates, especially for the mold with complex cavity.

Heat transfer in the mold

In conventional injection molding, the continuous cooling method is used by circulating the coolant in cooling channels during the whole molding cycle. As a consequence, cooling and solidification of the hot polymer melt begin as soon as the hot resin melt contacts with the cold mold cavity surfaces. Thus, the cooling process is coupled with filling and packing processes. However, mold temperature in RHCM is dynamically controlled by rapidly heating the mold before filling process, maintaining its high temperature during filling and packing processes,

then rapidly cooling it after packing. With such dynamic mold temperature control strategy, the cooling process is decoupled with filling and packing processes. Therefore, heat transfer in RHCM is quite different from that in conventional injection molding. In the following, we will mainly focus on heat transfer in heating and cooling stages of RHCM with electric heating. To facilitate discussion, heat transfer in filling and packing stages of RHCM will be neglected as filling and packing times are usually very short by contrasting with heating and cooling times.

Heat transfer in heating stage

In heating stage, heat generated by the heating elements, heating rods in this study, transfers through the interfaces of the heating rods and the mold steel, and then is conducted in the floating cavity/core. In heat transfer process, most of the generated heat energy accumulates in the mold steel and heating rods to raise their temperatures. Only a very small amount of heat diffuses into the ambient environment by convection and radiation. Figure 3 shows the heat transfer modeling of the heating stage. The instant energy balance of the heating stage in the floating cavity/core can be expressed by the following expression:

$$Q_g = Q_m + Q_h + Q_e \tag{1}$$

where Q_g is the heat generated by the heating elements; Q_m, Q_h represent the heat accumulations in the mold and heating rods, respectively; and Q_e denotes energy loss in the environment through the exterior of the mold. The generated heat energy, Q_g, is related to the heating elements' power, P_h and the required heating time, t_{reqh}.

$$Q_g = P_h \cdot t_{\text{reqh}} \tag{2}$$

If the mass, heat capacity, initial, and final average temperatures of the mold that needs to be heated are represented by the symbols of m_m, C_m, $\overline{T_{\text{mo}}}$, and $\overline{T_{\text{mf}}}$, respectively, heat accumulation, Q_m, in the mold can be expressed with the following equation:

$$Q_m = m_m \cdot C_m \cdot \left(\overline{T_{\text{mf}}} - \overline{T_{\text{mo}}}\right) \tag{3}$$

In a similar way, the heat accumulation, Q_h, in the heating rods can be expressed by the following equation:

$$Q_h = m_h C_h \cdot \left(\overline{T_{\text{hf}}} - \overline{T_{\text{ho}}}\right) \tag{4}$$

where m_h, C_h, $\overline{T_{\text{hf}}}$, and $\overline{T_{\text{ho}}}$ represent the mass, heat capacity, final, and initial average temperatures of the heating rod. The energy loss, Q_e, through the exterior surfaces of the mold can be approximately expressed by the following equation:

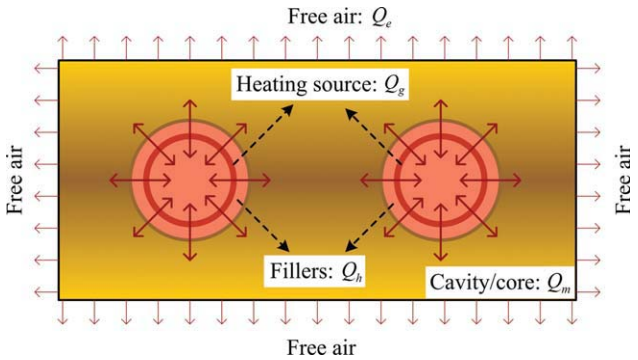

Figure 3 Heat transfer modeling of the heating stage. [Color figure can be viewed in the online issue, which is available at wileyonlinelibrary.com.]

$$Q_e = \alpha_e \cdot A_{\text{ms}} \cdot \int_0^{t_{\text{reqh}}} \left(\overline{T_m}(t) - T_e\right) dt \tag{5}$$

where α_e is the heat transfer coefficient at the mold exterior surfaces; A_{ms} represents the total area of the mold exterior surfaces; $\overline{T_m}(t)$ represents the average temperature of the mold at the heating time, t; and T_e is the environmental temperature. As the mold temperature increases nearly linearly with the increase of heating time,[17] eq. (5) can be changed into the following equation by solving the integral term.

$$Q_e = \frac{1}{2} \cdot \alpha_e \cdot A_{\text{ms}} \cdot \left(\overline{T_{\text{mf}}} - T_e\right) \cdot t_{\text{reqh}} \tag{6}$$

By submitting eqs (2)–(4) and (6) into eq. (1), the following expression can be obtained.

$$\begin{aligned} t_{\text{reqh}} \cdot P_h &= m_m \cdot C_m \cdot \left(\overline{T_{\text{mf}}} - \overline{T_{\text{mo}}}\right) + m_h \cdot C_h \cdot \left(\overline{T_{\text{hf}}} - \overline{T_{\text{ho}}}\right) \\ &\quad + \frac{1}{2} \cdot \alpha_e \cdot A_{\text{ms}} \cdot \left(\overline{T_{\text{mf}}} - T_e\right) \cdot t_{\text{reqh}} \\ \Rightarrow t_{\text{reqh}} &= \frac{m_m \cdot C_m \cdot \left(\overline{T_{\text{mf}}} - \overline{T_{\text{mo}}}\right) + m_h \cdot C_h \cdot \left(\overline{T_{\text{hf}}} - \overline{T_{\text{ho}}}\right)}{P_h - \frac{1}{2} \cdot \alpha_e \cdot A_{\text{ms}} \cdot \left(\overline{T_{\text{mf}}} - T_e\right)} \end{aligned} \tag{7}$$

As the whole surfaces of the floating cavity and core are surrounded by the good insulation material of free air during heating, heat loss through the exterior surfaces of the floating cavity and core is very little.[24] As a consequence, eq. (7) can be simplified into the following expression by neglecting the energy loss term:

$$t_{\text{reqh}} = \frac{m_m \cdot C_m \cdot \left(\overline{T_{\text{mf}}} - \overline{T_{\text{mo}}}\right) + m_h \cdot C_h \cdot \left(\overline{T_{\text{hf}}} - \overline{T_{\text{ho}}}\right)}{P_h} \tag{8}$$

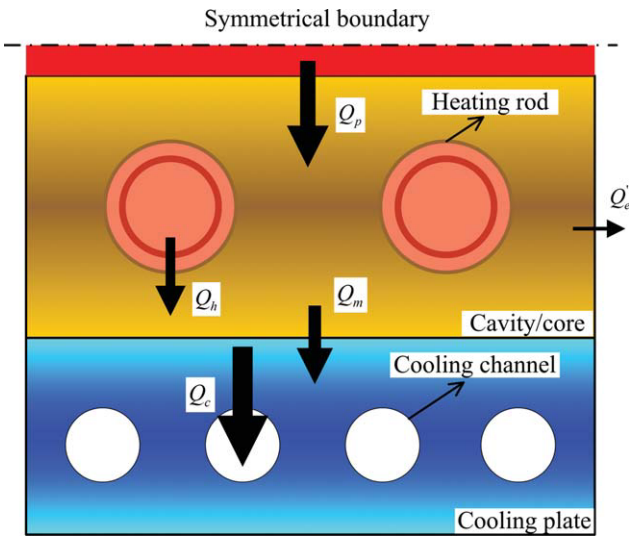

Figure 4 Heat transfer modeling of the cooling stage. [Color figure can be viewed in the online issue, which is available at wileyonlinelibrary.com.]

Generally, $\overline{T_{\mathrm{mj}}}$, $\overline{T_{\mathrm{hf}}}$, $\overline{T_{\mathrm{mo}}}$, and $\overline{T_{\mathrm{ho}}}$ are constant or change very little for specific polymer material and product. Therefore, the required heating time is mainly dependent upon the thermal mass (m_m, C_m, m_h, C_h) of the cavity/core and the heating rods, and also the power (P_h) of the heating rods. From the view of cavity/core material, metals with low heat capacity and density are much preferable to reduce thermal capacity of the floating cavity/core and hence decrease the required heating time. In addition, mold materials with high thermal conductivity also increase the heating rate of the mold cavity surface and decrease the required heating time by improving temperature distribution uniformity of the floating cavity/core. The common metals used as mold materials are including mold steel, aluminum, copper and their alloys. It is noteworthy that although copper or copper alloy has much high thermal conductivity than mold steel, thermal response efficiency of the copper mold is not necessarily higher than that of the steel mold because copper has much higher specific heat capacity and density than the steel mold. In other words, by comparing with mold steel, the positive effect of copper's higher thermal conductivity on thermal response efficiency of the mold could be offset by the negative effect of its larger thermal capacity on thermal response efficiency. Therefore, it is not surprising that the thermal response analysis results in previous study[17] show that the thermal response efficiency of the copper mold is a little smaller than that of the steel mold. In addition, volume reduction of the cavity/core is also very helpful for heating efficiency improvement. From the view of heating elements, the higher their power is the shorter the required heating time and the lower their thermal mass is the higher the heating efficiency. However, the power and filler's thermal mass of the heating rods are restricted by the available resistance heating technology at present.

Heat transfer in cooling stage

In cooling stage, hot polymer and the floating cavity/core are rapidly cooled down by the cooling plates, in the cooling channels of which cooling water is circulated continuously. The typical heat path is that heat is transferred from the hot polymer to the cavity/core, then is conducted through the cavity/core to the cooling plates, and finally arrives at the cooling channels, where it is convected away by the circulating cooling water. Figure 4 shows the heat transfer modeling of the cooling stage. The heat balance for cooling stage can be expressed with the following equation:

$$Q_c + Q_e' = Q_p + Q_m + Q_h \tag{9}$$

where Q_c is the heat convected away by the cooling water; Q_e represents the heat exchange with the environment in cooling stage; Q_p, Q_m, Q_h are the heat from molten polymer, hot cavity/core and the heating rods, respectively. As discussed above, the heat exchange with external environment is very little and can be neglected. As a result, eq. (9) can be changed into the following expression:

$$Q_c = Q_p + Q_m + Q_h \tag{10}$$

The heat stored in the mold and the fillers of the heating rods, Q_m and Q_h, are generated by the heat wire of the heating rods in the heating process, as shown in eq. (1). If the heat exchange with the environment is neglected, the following equation can be obtained by submitting eq. (1) in to eq. (10).

$$Q_c = Q_p + Q_g \tag{11}$$

The heat from the molten polymer, Q_p, can be expressed as:

$$Q_p = m_{\mathrm{mp}} \cdot \left[\left(T_{\mathrm{mp}} - T_e \right) \cdot C_{\mathrm{mp}} + i_{\mathrm{mp}} \right] \tag{12}$$

where m_{mp}, T_{mp}, C_{mp}, i_{mp} are the mass, temperature, heat capacity, and latent heat of the molten polymer; T_e is the ejection temperature of the polymer. The heat exchange with the cooling water in the required cooling time, t_{reqc}, can be calculated by the following formula.[25]

$$Q_c = t_{\text{reqc}} \cdot \left(\frac{1}{\lambda_c \cdot S_e} + \frac{1}{\alpha \cdot \pi \cdot d_c}\right)^{-1} \cdot L_c \cdot (T_w - T_{\text{cw}}) \quad (13)$$

where λ_c is the thermal conductivity of the cooling plate; S_e is the shape factor for the cooling channels; α is the heat transfer coefficient at the wall of the cooling channel; d_c is the diameter of the cooling channel; L_c is the total length of the cooling channels; T_w, T_{cw} are the mold wall temperature right after complete filling and temperature of the cooling water, respectively.

By submitting eqs. (2), (12), and (13) into eq. (11), the following expression can be obtained.

$$\begin{aligned} &t_{\text{reqc}} \cdot \left(\frac{1}{\lambda_c \cdot S_e} + \frac{1}{\alpha \cdot \pi \cdot d_c}\right)^{-1} \cdot L_c \cdot (T_w - T_{\text{cw}}) \\ &= m_{\text{mp}} \cdot \left[(T_{\text{mp}} - T_e) \cdot C_{\text{mp}} + i_{\text{mp}}\right] + P_h \cdot t_{\text{reqh}} \Rightarrow t_{\text{reqc}} \\ &= \frac{\left\{m_{\text{mp}} \cdot \left[(T_{\text{mp}} - T_e) \cdot C_{\text{mp}} + i_{\text{mp}}\right] + P_h \cdot t_{\text{reqh}}\right\} \cdot \left(\frac{1}{\lambda_c \cdot S_e} + \frac{1}{\alpha \cdot \pi \cdot d_c}\right)}{L_c \cdot (T_w - T_{\text{cw}})} \end{aligned} \quad (14)$$

For specific polymer material and part, m_{mp}, T_{mp} C_{mp}, i_{mp}, and T_e are constant or change very little. In other words, the heat released by the molten polymer is nearly constant. As it can be concluded from eq. (14), the methods presented in the last section to shorten the heating time by optimizing the mold design are also helpful to reduce the required cooling time. For example, the required cooling time can also be shortened by reducing the thermal mass of the floating cavity/core. Besides, the required cooling time can also be shortened by increasing the thermal conductivity of the cooling plate, decreasing the temperature of the cooling water and optimizing the design of the cooling channels. Further, considering that the cooling plates are used to support the floating cavity/core in mold closing state and are mainly subjected to compressive stress, good conductive metals, such as aluminum, copper or their alloys, although with lower strength than mold steel, are feasible and preferable to be used to manufacture the cooling plates. By doing this, rapid and uniform cooling of the floating cavity/core can be achieved.

EXPERIMENTAL STUDY

Design of experiment

For successful application in mass production of RHCM with electric heating, the reasonable design of the floating cavity/core is very crucial for electric-heating RTR mold. In fact, some problems have been found in actual industrial production, including high energy consumption due to low heating efficiency, high detective rate due to nonuniform temperature distribution, and short mold service life due to low structural strength of the floating cavity. These problems are all associated with the structure of the floating cavity/core. Therefore, it is very necessary to optimize the design of the floating cavity/core so as to improve its thermal response efficiency, temperature uniformity, and thermal fatigue strength. For this reason, design of experiments (DOE) and response surface methodology (RSM) have been employed for mold optimization design. RSM, mainly developed based on central composite design (CCD), is effective for the modeling and analysis of problems in which the desired response is affected by several variables.[26] In this study, the design variables consist of the half distance between the walls of two adjacent heating rods (a), the distance from the wall of the heating rod to the mold surface (b), and the diameter of the heating rod (d). The power density of the heating rod was assumed to be a constant value of 30 W/cm^2. Three design parameters should make up a unique set to achieve the best performance of the electric-heating mold. For instance, the smaller the distance from the heating rod to the mold surface, the more rapidly the mold surface is heated and the shorter the heating time. However, the resulting large mold surface temperature variation can lead to part quality problems. Besides, as the distance decreases, the mold strength will be reduced, resulting in short service life of the floating cavity/core. The levels of the design variables were chosen based on the previous experience and engineering analysis. Table I shows the limits of the selected design variables. The required heating time, t_{reqh}, when the whole mold surfaces are heated up to the designated temperature, 120°C in this study, is used to evaluate the thermal response efficiency. The shorter the required heating time is, the higher the thermal response efficiency. The maximum temperature, T_{max}, of the mold surface, right after heating process, is used to evaluate the temperature uniformity of the mold. The lower the maximum temperature is, the more uniform the temperature distribution. In practical production, the most common failure mode for such electric-heating RTR mold with floating cavity/core is the fatigue fracture resulting from frequent heating and cooling. Thus,

TABLE I
Levels of the Design Variables

		Limits				
Design Variables	Units	−1.5	−1	0	1	1.5
a	mm	4.00	5.00	7.00	9.00	10.00
b	mm	3.00	4.00	6.00	8.00	9.00
d	mm	3.00	4.00	6.00	8.00	9.00

TABLE II
Experimental Design Matrix Based CCD and Experimental Results Based on FEA

	Design Variables			Results		
No.	*a* (mm)	*b* (mm)	*d* (mm)	t_{reqh} (s)	T_{max} (°C)	σ_{max} (MPa)
1	7 (0)	6 (0)	6 (0)	12.0553	132.79	541.35
2	9 (+1)	8 (+1)	4 (−1)	21.4307	128.185	537.06
3	7 (0)	6 (0)	6 (0)	12.0553	132.79	540.86
4	7 (0)	6 (0)	9 (+1.5)	9.5774	131.962	544.2
5	7 (0)	6 (0)	3 (−1.5)	16.0980	126.684	507.45
6	9 (+1)	8 (+1)	8 (+1)	16.4235	135.83	561.51
7	7 (0)	6 (0)	6 (0)	12.0553	132.79	540.33
8	5 (−1)	8 (+1)	4 (−1)	13.7493	121.589	532.28
9	4 (−1.5)	6 (0)	6 (0)	8.3788	123.709	520.37
10	10 (+1.5)	6 (0)	6 (0)	16.2072	144.836	551.09
11	7 (0)	9 (+1.5)	6 (0)	16.3002	124.907	562.48
12	5 (−1)	4 (−1)	4 (−1)	8.0391	129.777	499.78
13	7 (0)	6 (0)	6 (0)	12.0553	132.79	541.78
14	9 (+1)	4 (−1)	4 (−1)	13.3712	146.906	547.36
15	7 (0)	3 (−1.5)	6 (0)	8.2715	154.803	550.21
16	9 (+1)	4 (−1)	8 (+1)	11.3093	163.962	590.89
17	7 (0)	6 (0)	6 (0)	12.0553	132.789	542.14
18	5 (−1)	8 (+1)	8 (+1)	11.3407	124.228	562.83
19	5 (−1)	4 (−1)	8 (+1)	7.1516	138.251	519.56
20	7 (0)	6 (0)	6 (0)	12.0553	132.79	540.75

the maximum von-Mises stress, σ_{max}, resulting from thermal expansion right after heating process is used to evaluate the structural strength of the mold. The larger the maximum von-Mises stress is, the lower the thermal fatigue strength and the shorter the fatigue life of the electric-heating cavity/core. A central composite experimental design was used to design the experimental matrix. The design included three combinations including the axial (A), factorial (F), and center (C) points. The design variables were specified at five different levels, as listed in Table I. The factorial points coded as '−1' and '+1', axial points as '−1.5' and '+1.5' along with center point coded '0' were included in the experimental design. Table II lists the design matrix based on CCD.

Experiment based on finite element analysis

With the rapid development of solid freeform fabrication techniques, conformal cooling channels are available for injection molding to achieve uniform cooling and minimum molding cycle time.[27–29] By imitating the conformal cooling technique, conformal heating technique can also be used for the electric-heating RTR mold by placing the heating elements conforming to the surfaces of the mold cavity. As a result, heat transfer in the electric-heating mold is confined in the small region between two adjacent heating rods because of the structural symmetry.[28] Therefore, an individual cell unit, as shown in Figure 5, can be used to investigate the thermal response, temperature uniformity, and thermal fatigue strength of the electric-heating RTR mold. In Figure 5, symbols of *a*, *b*, *d* represent the half distance between the walls of two adjacent heating rods, the spacing from the wall of the heating rod to the mold surface and diameter of the heating rod, respectively. The spacing between the wall of the heating rod and the back surface of the cavity/core is equal to the distance from the wall of the heating rod to the mold surface.

The cavity/core material used in this study is the hot work steel (AISI H11), which has high level of thermal fatigue, good high-temperature strength, excellent toughness, and ductility in all directions and high corrosion resistance. The filler material of the heating rods is MgO–SiO_2. The thermal and mechanical properties of the mold steel and the fillers are listed in Table III.[30]

Heat transfer analysis and thermal stress analysis were conducted based on the commercial finite element analysis software, ANSYS, to investigate the thermal response and stress distribution of the cavity/core in heating process. Transient heat transfer analysis was firstly conducted to obtain the required heating time and temperature distribution when the whole mold surface is heated up to the designated temperature of 120°C. Then, a static structural analysis was conducted to obtain the stress distribution within the cavity/core right after heating process. Owing to the symmetrical structure of the cell unit model shown in Figure 5, quarter mesh models are employed for the following finite element analysis. Figures 6 and 7 shows the mesh models and boundary conditions for transient heat transfer analysis and static thermal stress analysis, respectively. For

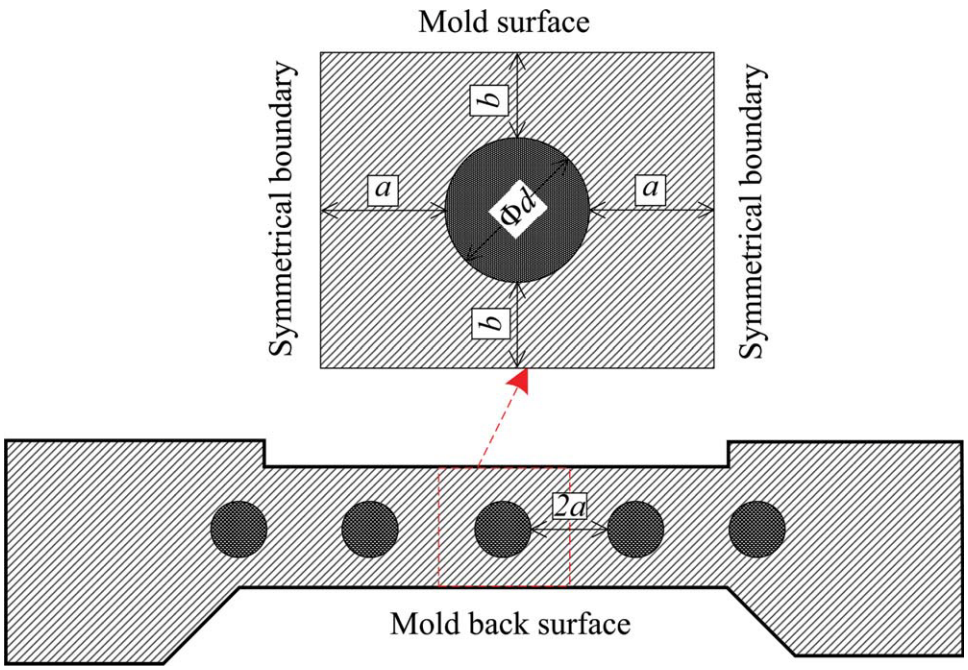

Figure 5 Sketch of an individual cell unit for thermal and structural analysis. [Color figure can be viewed in the online issue, which is available at wileyonlinelibrary.com.]

heat transfer analysis, the initial temperature of the cavity/core is assumed to be equal to the environmental temperature of 30°C. As shown in Figure 6, air free convection is loaded on the cavity surface and the back surface of the floating cavity/core. Considering the good ventilations in workshop, the convection coefficient on the exterior surfaces is assumed to be 15 $W/m^{2o}C$.[31] According to the power density of the available heating elements at present, the heat flux of 3.0×10^5 W/m^2 is loaded on the interface of the heating rod and the mold steel to simulate the heat generated by heating wires in the heating rod. In addition, a default boundary condition of adiabatic is automatically assigned on the symmetrical boundaries. For static structural analysis, the temperature results of transient heat transfer analysis right after the whole floating cavity surface is heated up to the designated temperature are loaded on the mesh model for structural analysis as initial temperature conditions. As shown in Figure 7, the top and bottom sides of the model are free surfaces with no constrains. The left and right sides of the model are loaded with symmetry boundary conditions and displacements along the norm direction of the two sides are restricted to be zero.

According to the experimental design plans listed in Table II, 20 sets of thermal response analysis and thermal–structural analysis were implemented to acquire the values of the three objective variables including required heating time, maximum temperature, and maximum von-Mises stress. The analysis results are recorded in Table II. Figure 8 shows the typical temperature response of the cavity surface in heating process. It can be seen that the cavity surface temperature increases very slowly and almost keep constant in the very short initial heating time, t_{con}, which is the so-called mold time constant and an indicator of the thermal response rate of the mold to external energy change.[21] However, the cavity surface temperature rises linearly with the increase of the heating time after the initial heating time of t_{con} As a result, the cavity surface temperature can be precisely controlled by indirectly controlling the heating time of the heating elements in practical production.

TABLE III
Thermal and Mechanical Properties of the Mold Steel and Heating Rod Fillers

Material	Density (kg/m^3)	Specific Heat (J/kg)	Thermal Conductivity (W/m °C)	Thermal Expansion Coefficient (μm/m °C)	Elastic Modulus (GPa)	Poisson's Ratio
AISI H11	7850	460	34	13	205	0.285
$MgO–SiO_2$	2700	1100	5.5	8.2	107	0.23

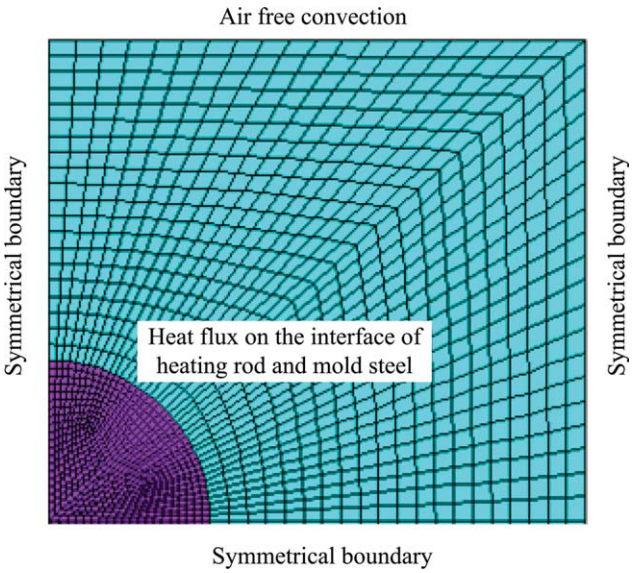

Figure 6 Mesh model and boundary conditions for transient heat transfer analysis. [Color figure can be viewed in the online issue, which is available at wileyonlinelibrary.com.]

CONSTRUCTION OF THE RESPONSE SURFACE MODELS

In this section, analysis of variance (ANOVA) was applied to summarize the experimental results for the response surface quadratic models. The mathematic models for three response variables, which were used to evaluate thermal response efficiency, temperature uniformity and structural strength of the mold, were created by experimental design technique and regression analysis. ANOVA, "*F*-value," "*P*-value" of the statistical parameters were used to test the significance of the parameters and the adequacy of the regression models. Test experiments were also conducted to check the accuracy of the developed prediction models.

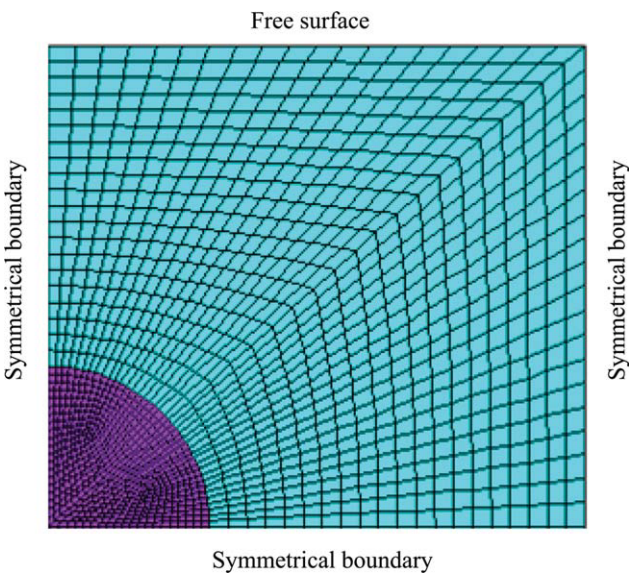

Figure 7 Mesh model and boundary conditions for static thermal stress analysis. [Color figure can be viewed in the online issue, which is available at wileyonlinelibrary.com.]

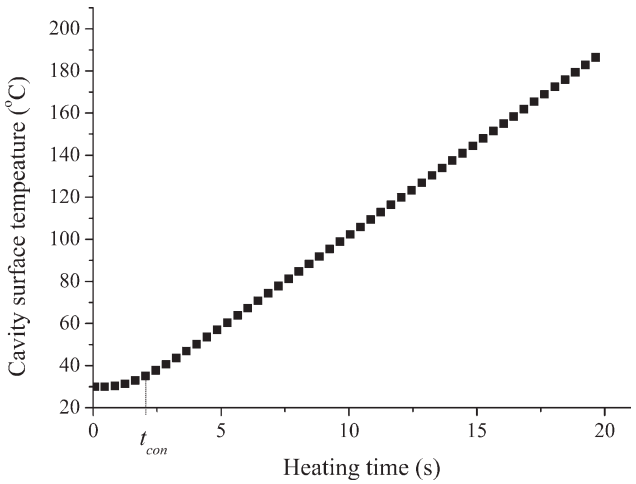

Figure 8 Typical temperature response of the cavity surface in heating process.

ANOVA results

The ANOVA results of the quadratic model for required heating time are presented in Table IV. Both "*F*-value" and "*P*-Value" of the statistical parameters were used to confirm the significance of the terms investigated.[32] The "*F*-value" was calculated from a model mean square divided by a residual mean square. It is a test that compares a term variance with a residual variance. If the variances are close to the same, the ratio will be close to one and the corresponding term is less likely to have a significant effect on the response variable. In addition, the design term with "*P*-value" less than 0.05 demonstrate that it has a significant effect on the response variables. In the same manner, an "*F*-value" of 87.56 and a "*P*-value" of less than 0.0001 for the model of required heating time, as given in Table IV, indicate that the model is very significant. In addition, the single terms of *a*, *b*, *d* interaction terms of *ad*, *bd*, and quadratic terms of d^2 are the significant factors associated with the required heating time. In other words, the thermal response efficiency of the electric-heating cavity/core is mainly dependent on these design terms. Similar to the ANOVA analysis of the model of required heating time, ANOVA results for the other two models of maximum cavity surface temperature and maximum von-Mises stress right after heating process are given in Tables V and VI, respectively. An "*F*-value" of 76.08 and a "*P*-value" of less than 0.0001 for the maximum cavity surface temperature, and an

TABLE IV
ANOVA Results for the Required Heating Time

Source	Sum of Squares	DOF	Mean Square	*F*-Value	*P*-Value
Model	228.715	9	25.41278	87.55834	<0.0001
a	89.54753	1	89.54753	308.5311	<0.0001
b	98.65096	1	98.65096	339.8965	<0.0001
d	32.46923	1	32.46923	111.8709	<0.0001
ab	1.340212	1	1.340212	4.617627	0.0572
ad	1.779441	1	1.779441	6.130967	0.0328
bd	2.493591	1	2.493591	8.591532	0.0150
a^2	0.548861	1	0.548861	1.891071	0.1991
b^2	0.224514	1	0.224514	0.77355	0.3998
d^2	1.590625	1	1.590625	5.480413	0.0413
Residual	2.902382	10	0.290238		
Total	231.62	19			

"*F*-value" of 31.45 and a "*P*-value" of less than 0.0001 for the maximum von-Mises stress demonstrate that both of the two models are significant. For the model of the maximum cavity surface temperature, the single term of *a*, *b*, *d*, interaction terms of *ab*, *bd*, along with the quadratic terms of b^2 and d^2 are significant factors. For the model of the maximum von-Mises stress, the single term of *a*, *b*, *d* interaction terms of *ab*, along with the quadratic terms of b^2 and d^2 are significant factors.

Regression for response surface models

To predict the objective variables with different design variables in the design space, second-order polynomial equations were fitted to create the numerical relationships between the variables and responses. By involving in all the single, quadratic, and interaction terms, the typical polynomial equation for the quadratic response model can be written as:

$$Y = \beta_0 + \sum_{i=1}^{i=k} \beta_i X_i + \sum_{i<j}^{k} \beta_{ij} X_i X_j + \sum_{i=1}^{k} \beta_{ii} X_i^2 \qquad (15)$$

where Y represents the response variable; β_0 is the model constant; k is the number of the design variables; β_i is the linear coefficient of the design variable X_i; β_{ij} is the interactive coefficient for the design variables of X_i and X_j; and β_{ii} is the quadratic coefficient of the design variable of X_i. Based on the experimental results, the mixed regression method was used to estimate the unknown coefficients of β_0, β_i, β_{ij}, and β_{ii}. The fitting response surface mathematical models describing the required heating time, maximum cavity surface temperature and von-Mises stress right after heating process are given in eqs. (16)–(18), respectively.

$$t_{\text{reqh}} = 1.08641 + 0.62404a + 1.08302b - 0.32164d + 0.10233ab - 0.11791ad - 0.13957bd + 0.057694a^2 + 0.036900b^2 + 0.098216d^2 \qquad (16)$$

$$T_{\max} = 123.19798 + 2.45075a - 6.60575b + 5.37967d - 0.77006ab + 0.42463ad - 0.47644bd + 0.23793a^2 + 0.85821b^2 - 0.31201d^2 \qquad (17)$$

$$\sigma_{\max} = 314.75191 + 28.43632a + 4.38665b + 20.72196d - 3.60781ab + 0.55156ad - 0.25969bd - 0.24006a^2 + 2.05050b^2 - 1.34061d^2 \qquad (18)$$

TABLE V
ANOVA Results for the Maximum Cavity Surface Temperature

Source	Sum of Squares	DOF	Mean Square	*F*-Value	*P*-Value
Model	2153.021	9	239.2246	76.07796	<0.0001
a	687.886	1	687.886	218.7608	<0.0001
b	1038.003	1	1038.003	330.1045	<0.0001
d	152.992	1	152.992	48.65437	<0.0001
ab	75.90352	1	75.90352	24.13876	0.0006
ad	23.07922	1	23.07922	7.33963	0.0220
bd	29.05506	1	29.05506	9.240062	0.0125
a^2	9.334684	1	9.334684	2.968607	0.1156
b^2	121.4469	1	121.4469	38.62243	<0.0001
d^2	16.05283	1	16.05283	5.105106	0.0474
Residual	31.44466	10	3.144466		
Total	2184.47	19			

TABLE VI
ANOVA Results for the Maximum von-Mises Stress

Source	Sum of Squares	DOF	Mean Square	*F*-Value	*P*-Value
Model	7609.932	9	845.548	31.4458	<0.0001
a	2270.032	1	2270.032	84.42215	<0.0001
b	237.5764	1	237.5764	8.83543	0.0140
d	2406.376	1	2406.376	89.49275	<0.0001
ab	1666.088	1	1666.088	61.96155	<0.0001
ad	38.94031	1	38.94031	1.448184	0.2565
bd	8.632012	1	8.632012	0.321023	0.5835
a^2	9.502458	1	9.502458	0.353395	0.5654
b^2	693.2983	1	693.2983	25.78366	0.0005
d^2	296.353	1	296.353	11.02132	0.0077
Residual	268.8906	10	26.88906		
Total	7878.82	19			

Accuracy check for regression models

Before using the developed mathematical models to predict the response variables in the design space, it is very necessary to check the accuracy of these models. The normal probability plots of the residuals for the required heating time, maximum cavity surface temperature and maximum von-Mises stress are shown in Figure 9. It can be observed that the residuals for all the response variables fall on a straight line. This demonstrates that the errors are distributed normally and it is adequate to obtain multiple regression coefficients by employing the least squares technique. In addition, three confirmation experiments were conducted with design variables chosen randomly within the design space to validate the developed response surface models. Table VII gives the random data sets for check and the comparison of the calculation results by the quadratic polynomial models and numerical experiments based on FEA. It can be found that the maximum absolute relative errors for the three response variables between the estimated results and the experimental results are 2.73, 0.585, and 1.48%, respectively. Such small errors indicate that the developed polynomial models are adequate and can be used to predict the objective variables with good accuracy in the design space.

OPTIMIZATION BY PARTICLE SWARM ALGORITHM

Optimization model

From the prospective of molding production, it is desired to maximize heating efficiency, minimize cavity surface temperature difference and maximize mold strength to achieve the highest productivity, highest quality products, and longest mold lifetime. However, it is impossible to meet all of the requirements at the same time because these objective variables conflict with each other. In fact, the process requirements for heating efficiency, cavity surface temperature uniformity, and mold lifetime vary for different types of plastic products. For instance, the optic parts require much more uniform cavity surface temperature to achieve uniform optical properties. However, it should be given more attention on mold strength for the great mass-produced parts to ensure an adequate service life of the electric-heating RTR mold. It would be very time-consuming and hence greatly increase production cost if the mold is damaged prematurely. In addition, the conception that the heating time should be as short as possible is not always right in any case. In fact, the heating process has no effect on the whole molding cycle as long as the required heating time does not exceed the total time for norm mold opening and closing.[2] By comprehensively considering these different cases, three different optimization strategies including heating efficiency priority, temperature uniformity priority and mold strength (or thermal fatigue strength) priority are chosen in this study. The purpose of heating efficiency priority is to minimize the required heating time. At the same time, the maximum cavity surface temperature and von-Mises stress right after heating must be not more than 125°C and 540 MPa, respectively. The corresponding optimization mathematical model can be defined by the following expression.

$$\begin{aligned}
&\text{Find}: \ a,\ b,\ d\\
&\text{Minmize}: \ t_{\text{reqh}}(a,\ b,\ d)\\
&\text{Subjected to constraints}:\\
&T_{\max}(a,\ b,\ d) \le 125^{\circ}\text{C and } \sigma_{\max}(a,\ b,\ d) \le 540\ \text{MPa}\\
&\text{Within ranges}:\\
&5\ \text{mm} \le a \le 9\ \text{mm},\ 4\ \text{mm} \le b \le 8\ \text{mm and}\\
&\qquad 4\ \text{mm} \le d \le 8\ \text{mm} \qquad (19)
\end{aligned}$$

For the optimization strategy of temperature uniformity priority, the purpose is to minimize the

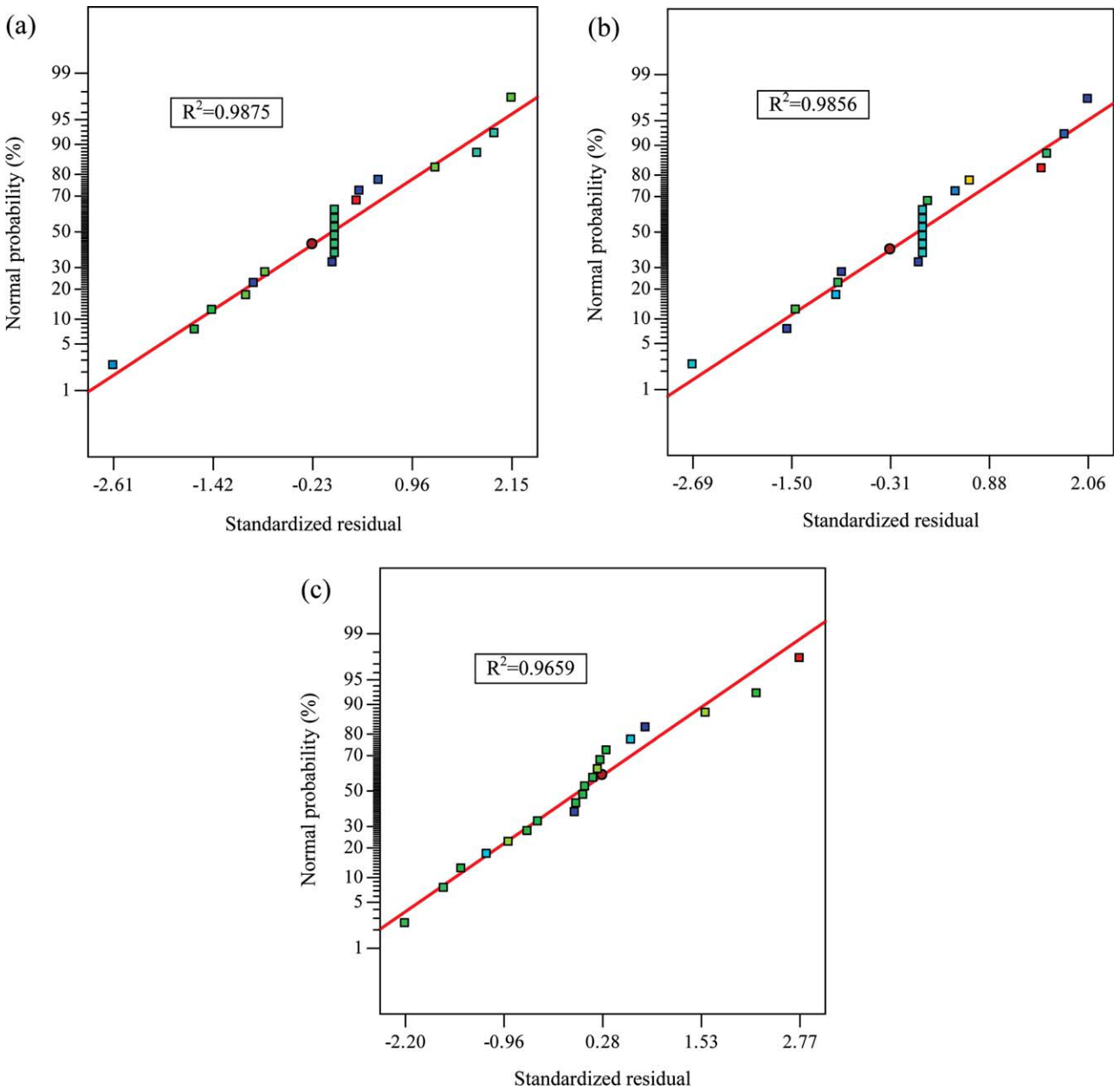

Figure 9 Normal probability plot residuals for (a) required heating time, (b) maximum cavity surface temperature, and (c) maximum von-Mises stress. [Color figure can be viewed in the online issue, which is available at wileyonlinelibrary.com.]

TABLE VII
Comparison of the Results Obtained by the Developed Quadratic Polynomial Models and Numerical Experiments with Random Design Variables

No.	*a* (mm)	*b* (mm)	*d* (mm)		t_{reqh} (s)	T_{max} (°C)	σ_{max} (MPa)
1	8	7	7	Predicted	14.0101	133.523	553.55
				Experimental	14.1956	134.309	561.84
				Error (%)	−1.31	−0.585	−1.48
2	6	7	5	Predicted	13.0197	125.099	533.93
				Experimental	12.7549	125.312	531.07
				Error (%)	2.08	−0.170	0.539
3	8	5	7	Predicted	11.2751	145.219	556.92
				Experimental	11.5916	145.252	561.11
				Error (%)	−2.73	−0.0227	−0.746

maximum cavity surface temperature, in other words, minimize the maximum temperature difference on the cavity surface. After optimization, the required heating time must be less than 12 s and the maximum von-Mises stress right after heating must be not more than 540 MPa. The corresponding optimization mathematical model is given as the following expression.

$$\begin{aligned}&\text{Find}: \ a,\ b,\ d\\&\text{Minmize}: \ T_{\max}(a,\ b,\ d)\\&\text{Subjected to constraints}:\\&t_{\text{reqh}}(a,\ b,\ d) \le 12\ \text{s and}\ \sigma_{\max}(a,\ b,\ d) \le 540\ \text{MPa}\\&\text{Within ranges}:\\&5\ \text{mm} \le a \le 9\ \text{mm},\ 4\ \text{mm} \le b \le 8\ \text{mm and}\\&\qquad 4\ \text{mm} \le d \le 8\ \text{mm}\end{aligned} \quad (20)$$

For the optimization strategy of mold strength priority, it is expected to minimize the maximum von-Mises stress so as to maximize the thermal fatigue life of the floating electric-heating cavity/core. To ensure a reasonable heating efficiency and temperature uniformity, the required heating time and the maximum von-Mises stress should not be more than 12 s and 125°C, respectively. The corresponding optimization mathematical model for this optimization strategy can be expressed by the following expression.

$$\begin{aligned}&\text{Find}: \ a,\ b,\ d\\&\text{Minmize}: \ \sigma_{\max}(a,\ b,\ d)\\&\text{Subjected to constraints}:\\&t_{\text{reqh}}(a,\ b,\ d) \le 12\ \text{s and}\ T_{\max}(a,\ b,\ d) \le 125^{\circ}\text{C}\\&\text{Within ranges}:\\&5\ \text{mm} \le a \le 9\ \text{mm},\ 4\ \text{mm} \le b \le 8\ \text{mm and}\\&\qquad 4\ \text{mm} \le d \le 8\ \text{mm}\end{aligned} \quad (21)$$

Optimization problem solution based on PSO

Particle swarm optimization (PSO) is a population-based stochastic optimization technique developed by Kennedy and Eberhart in 1995,[33,34] inspired by social behavior of organisms such as bird flocking and fish schooling. Contrasting with other methods such as genetic algorithms (GA) and evolutionary algorithms (EA), it supplies a much faster and cheaper way for solving complex optimization problems. In recent years, it has been successfully applied in many research and application areas.[35–37] As an optimization procedure, PSO is based on the velocity-position searching model by combing the local and global optimization methods. At the beginning of PSO, a set of potential solutions called particles are initialized in the design space. After each time iteration step, each particle updates its velocity and position by dynamic tracking two best solutions. One is the optimal solution that each particle has achieved so far by that particle. This optimal solution is called personal best value, pbest. The other one is the optimal solution achieved for the particle swarm after current iterations. This optimal solution is called the group best value, gbest. During iterations, the fitness function is used to decide the performance of the solutions after each iteration step. The velocity and position updates of the particle are according to the following equations.

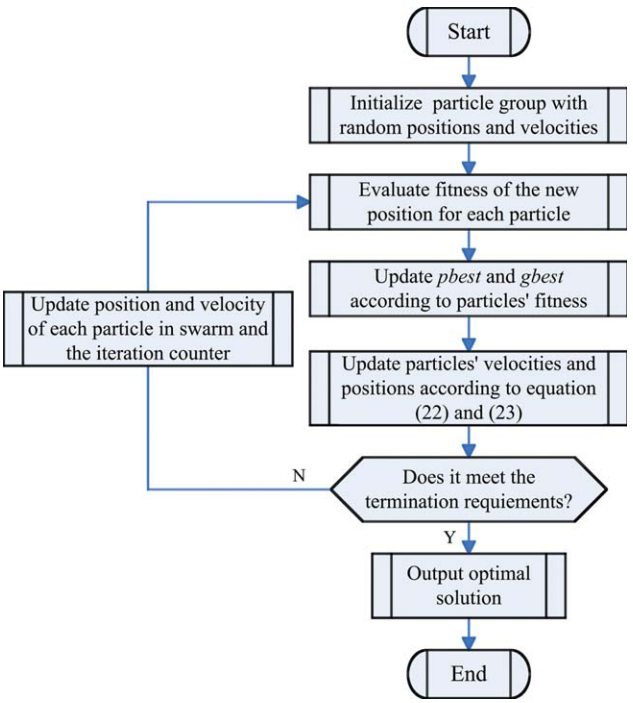

Figure 10 Flow chart depicting the general PSO algorithm. [Color figure can be viewed in the online issue, which is available at wileyonlinelibrary.com.]

$$v_i^{k+1} = \omega \cdot v_i^k + c_1 \cdot \text{rand}_1() \cdot \left(\text{pbest}_i - s_i^k\right) + c_2 \cdot \text{rand}_2() \cdot \left(\text{gbest} - s_i^k\right) \quad (22)$$

$$s_i^{k+1} = s_i^k + v_i^{k+1} \quad (23)$$

where v_i^k, v_i^{k+1} are the velocities of particle i at iteration of k and $k + 1$, respectively; s_i^k, s_i^{k+1} represent the displacements of particle i at iteration of k and $k + 1$, respectively; ω is the weighting function; c_1, c_2 are the study factors; pbest_i is the pbest of particle i; $\text{rand}_1()$, $\text{rand}_2()$ are the random numbers between 0 and 1. Figure 10 shows the flow chart depicting the general PSO algorithm.

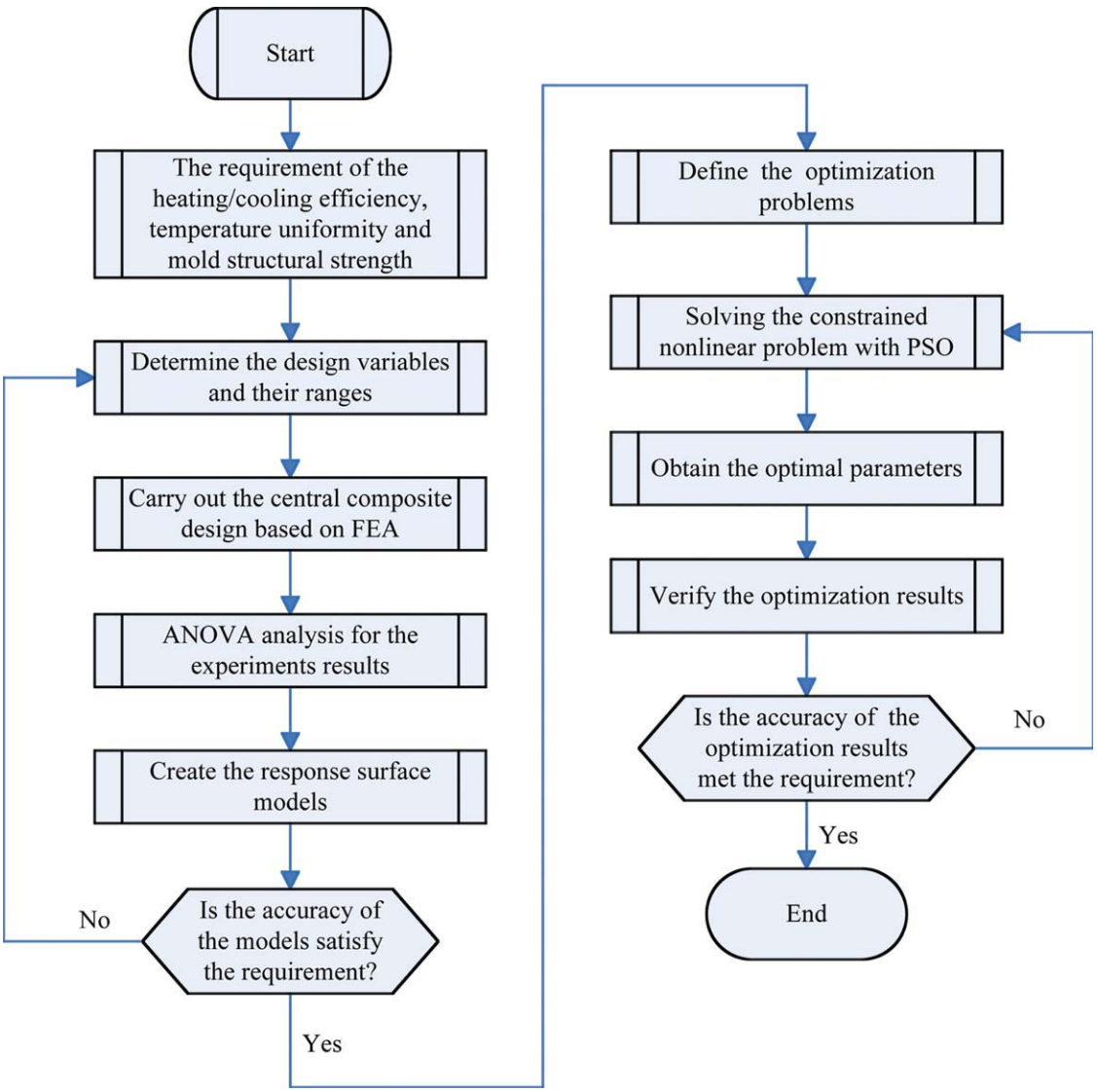

Figure 11 The flow chart of optimization design. [Color figure can be viewed in the online issue, which is available at wileyonlinelibrary.com.]

The flow chart of the layout optimization design of the heating elements in the floating cavity/core is shown in Figure 11. Firstly, the numerical relationships between design variables and objective variables are constructed by experiment design and numerical experiments based on FEA. Secondly, quadratic response surface mathematical models are created by ANOVA and regression analysis. Finally, the defined nonlinear and constraint multiobjective optimization problems expressed by eqs. (19)–(21) were solved by the developed PSO algorithm. MATLAB programming language was used to write the PSO algorithm. In this study, a linear decreasing function was used as the weighting function, ω, in eq. (22) and its initial and final valves reduce linearly from 0.9 to 0.4 with the increase of iteration number. In addition, the study factors, c_1 and c_2 in eq. (22), were both assumed to be 1.4962.

Optimization results and verification

Based on the developed PSO algorithm, the optimization problems defined by expressions (19–21) were solved. Figure 12 shows the optimization histories with iterations for the three different optimization strategies presented above. The optimal results are listed in Table VIII. The numerical experiments with the optimal design parameters were also performed to validate the optimal results. The data obtained from the confirmation experiments based on FEA and their comparisons with the optimal results are given in Table VIII. It can be observed in Table VIII that the percentage errors calculated for all cases are very small. The ranges of percentage error between the experimental and optimal values of required heating time, maximum cavity surface temperature, and maximum von-Mises stress lie within −3.72 to 3.08%, −1.79 to 0.311%, and −0.789 to −0.0775%, respectively.

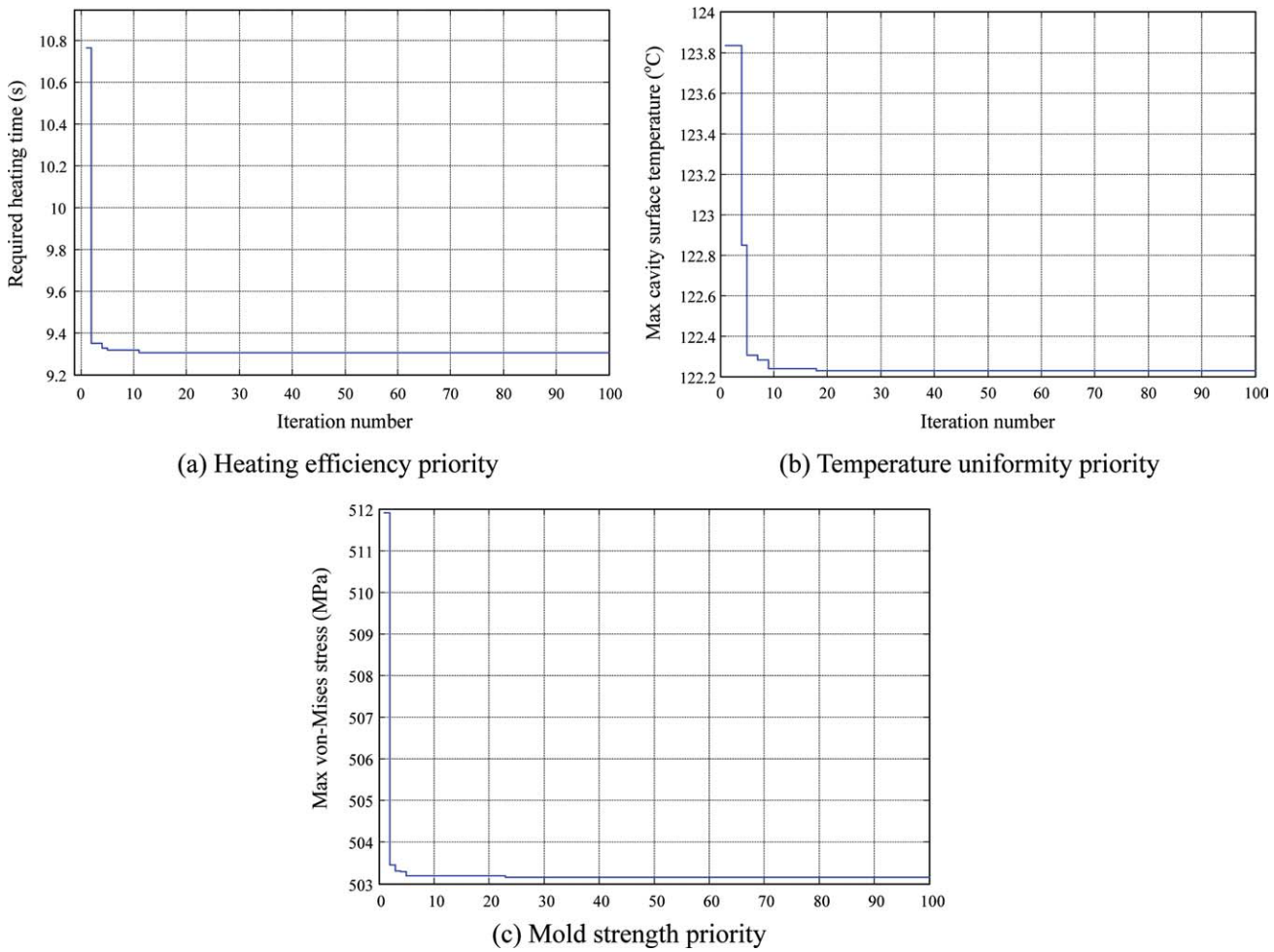

Figure 12 Optimization histories with iterations for (a) heating efficiency priority, (b) temperature uniformity priority, and (c) mold strength priority. [Color figure can be viewed in the online issue, which is available at wileyonlinelibrary.com.]

APPLICATION IN MOLD DESIGN

In this part, the electric-heating RTR mold with a floating cavity for an actual industrial product of the LCD TV frame was taken as an example to discuss the application of the presented optimization mold design method. Figure 13 shows the model of the LCD TV frame and its four typical cross-section views. As the inner surface of the frame is invisible after assembly, only the outer surfaces of the part are required to be with high glossy surface and without surface defects, such as weld line and flow mark. As a result, only the cavity side of the LCD TV frame mold should be thermally cycled by rapid heating and cooling to dynamically control its cavity surface temperature. Electric heating rods distributed conformally to the floating cavity surfaces are used to heat the floating cavity, which has thin thickness and can move forward and backward in injection molding process. The developed optimization method based on RSM and PSO was used to optimize the layout of the heating rods in the floating cavity.

Figure 14 shows the basic plan for the placement of the heating rods. Firstly, the part line is established according to the section view of the 3D model of the LCD TV frame. Secondly, the heating rod line and cavity back surface line are established by creating equidistance lines based on the part line. The offset distance between heating rod line and part line is the same as that between the cavity back surface line and the heating rod line. The offset distance is equal to the sum of the heating rod's radius, $d/2$, and the distance from the wall of the heating rods to the cavity surface line, b. Finally, the position of the heating rods can be determined by distribute the heating rods uniformly on the heating rod line with the same spacing between each other, $2 \times a$. Owing to the size restriction of available heating rods in this study, the heating rods with the diameter of 6 mm were used. In addition, the developed optimization method was used to determine the optimal values of a and b. Taking productivity into account for large mass production of the LCD TV frame, the first

TABLE VIII
Comparisons of the Optimal Results Based on PSO and the Experimental Verification Results Based on FEA

Optimization Strategy	a (mm)	b (mm)	d (mm)		t_{reqh} (s)	T_{max} (°C)	σ_{max} (MPa)
Heating efficiency priority	5.00	6.49	8.00	Optimal	9.3035	125.000	537.27
				Experimental	9.6630	127.282	541.54
				Error (%)	−3.72	−1.79	−0.789
Temperature uniformity priority	5.00	6.58	4.00	Optimal	12.0000	122.231	515.57
				Experimental	11.6416	123.003	515.97
				Error (%)	3.08	−0.628	−0.0775
Mold strength priority	5.00	5.30	4.00	Optimal	10.1086	125.000	503.16
				Experimental	9.8023	125.390	505.03
				Error (%)	2.94	−0.311	−0.370

optimization strategy of heating efficiency priority was selected. The optimal results are $a = 5$ mm and $b = 6.45$ mm. With the optimal design parameters, the layout of the heating rods and all the four cross-section shapes of the cavity can be determined. Based on the optimal cross-section shapes, the three-dimensional structure of the cavity can be constructed. Figure 15 shows the 3D model of the cavity

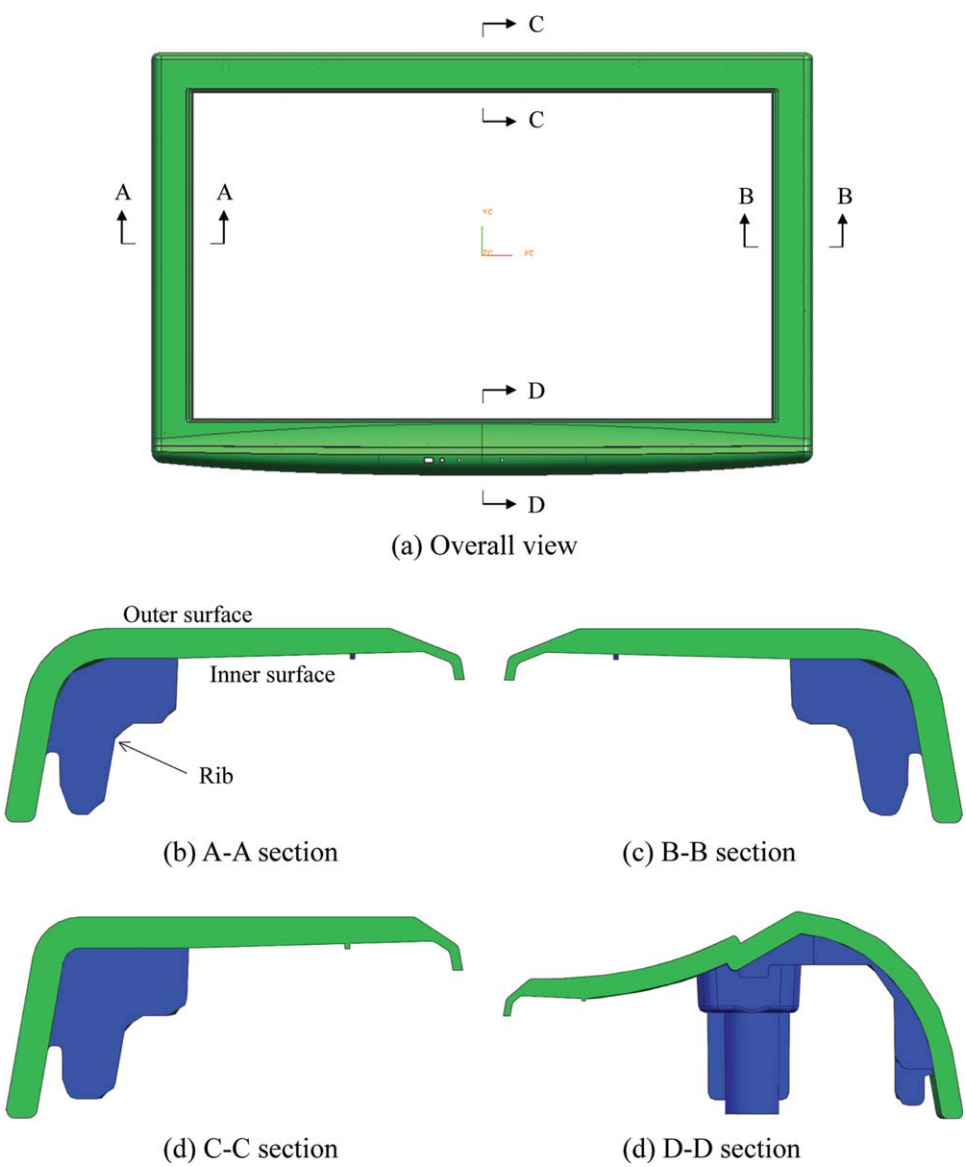

Figure 13 The model of a LCD TV frame and its four typical cross-section views. [Color figure can be viewed in the online issue, which is available at wileyonlinelibrary.com.]

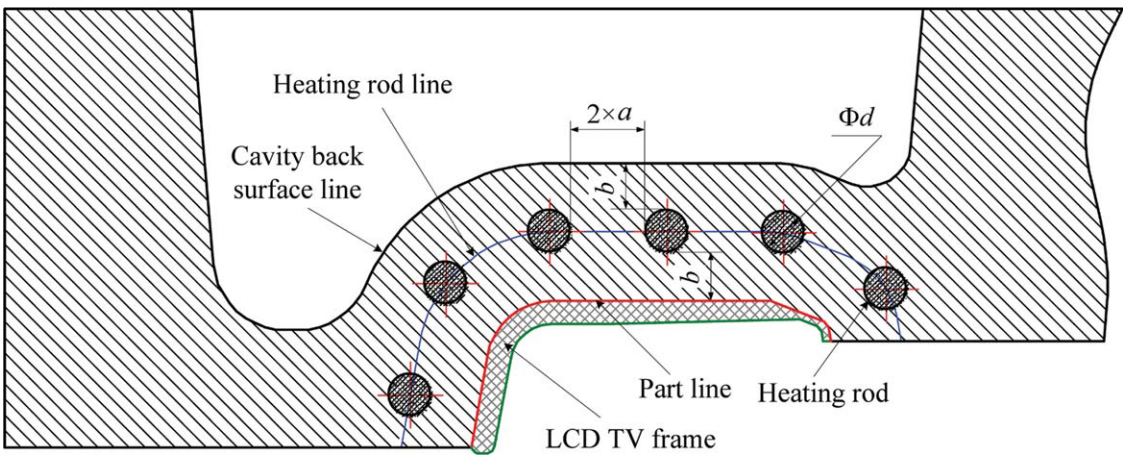

Figure 14 The basic plan for the layout of the heating rods. [Color figure can be viewed in the online issue, which is available at wileyonlinelibrary.com.]

and the layout of the heating rods. As shown in Figure 15, it is noteworthy that some stiffening ribs are preserved to improve the strength and rigidity of the floating cavity. However, Tthe thickness of the stiffening rib should not be too thick. Otherwise, it will reduce thermal response efficiency of the floating cavity due to the increase of the cavity volume and also lead to nonuniform temperature distribution.

To verify the effectiveness of the optimal structure and heating rods layout of the floating cavity, heat transfer analysis based on FEA for the optimal design case and original design case were both performed. Figure 16 shows the 2D heat transfer analysis models for the optimal and original design cases. The thermal properties of the cavity and heating rods have been presented in Table III. Analysis condition settings for heat transfer analysis are omitted here, as they have been detailed in our previous study.[2] Figure 17 shows the contour plots of temperature distributions in the cavity before and after optimizations when most of the cavity surfaces have been heated up to the required temperature of 120°C. It can be found that the optimal design case has much more uniform temperature distribution on the cavity surface than the original design case. Although most of the middle regions of the cavity surface for the original design case have been raised up to be higher than 120°C, the cavity surface

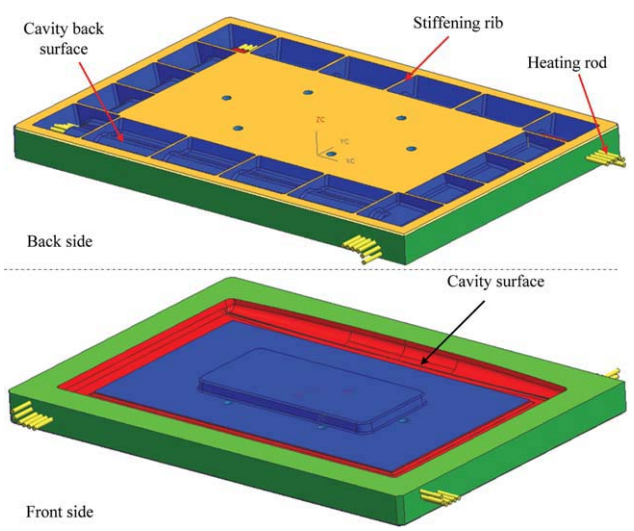

Figure 15 The 3D model of the cavity and the layout of the heating rods. [Color figure can be viewed in the online issue, which is available at wileyonlinelibrary.com.]

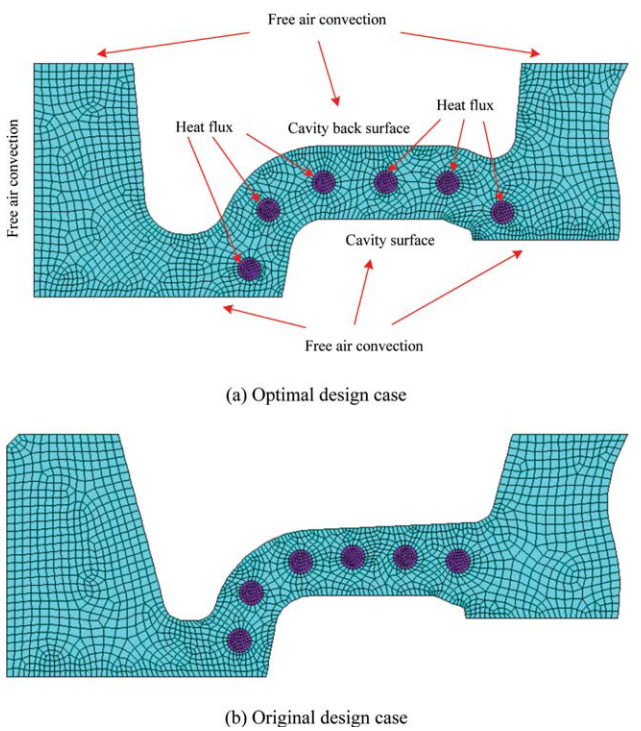

Figure 16 Mesh models and boundary conditions of heat transfer analysis for (a) optimal design case and (b) original design case. [Color figure can be viewed in the online issue, which is available at wileyonlinelibrary.com.]

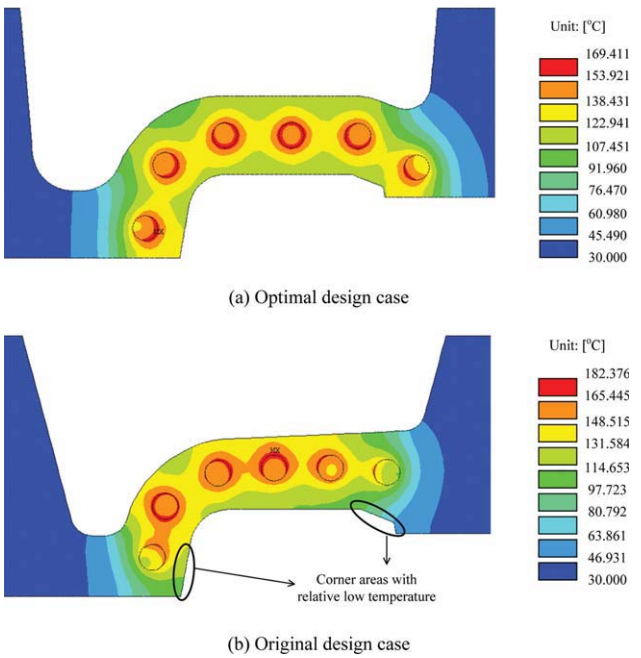

Figure 17 Temperature distributions in the cavity for (a) optimal design case and (b) original design case. [Color figure can be viewed in the online issue, which is available at wileyonlinelibrary.com.]

temperatures at the corner areas are still much lower than 120°C. This can be seen much more clearly in Figure 18 that shows the comparison of temperature distributions on the cavity surface for the two design cases. It can be observed that the maximum temperature difference for the optimal design case is only about 10°C while the maximum temperature difference for the original design case is larger than 80°C. As a result, it could be concluded that the final product for the optimal design case has much better and more uniform surface appearance, lower inner stress, and better mechanical properties due to its much more uniform temperature distribution. In addition, the uniform temperature distribution in the cavity can also reduce thermal stress caused by thermal expansion. Accordingly, the thermal fatigue life of the cavity can be improved. It is therefore reasonable to conclude that the electric-heating mold in the optimal design case has longer thermal fatigue life than that in the original design case. This means the optimal design case can also improve the service life of the electric-heating RTR mold with floating cavity.

CONCLUSIONS

This study discusses a new RHCM process with electric heating and coolant cooling. A new electric-heating RTR mold structure with floating cavity/core and separate cooling plates was presented. The factors affecting heating and cooling efficiencies of the electric-heating mold were investigated. Some potential useful design principles to improve thermal response efficiency were proposed by deriving heat balance equations in the RTR molding systems.

Response surface methodology based on CCD and FEA simulation were utilized to create the numerical relationships between heating systems parameters and the heating efficiency, temperature uniformity, and thermal fatigue strength of the electric-heating cavity/core. The corresponding quadratic response surface models were developed for prediction of the objective parameters by regression analysis. The reliabilities and accuracies of the developed mathematic models were verified by ANOVA analysis and validation experiments. With the developed mathematic models, three different optimization strategies including heating efficiency priority, temperature uniformity priority, and mold strength priority were proposed and the corresponding optimization mathematic models were also created. An efficient optimization methodology by integrating the response mathematic models and PSO algorithm was developed to solve the constraint multiobjectives optimization problems. Optimization results show that the optimal design parameters for the three optimization strategies are (a = 5.00 mm, b = 6.49 mm, d = 8.00 mm), (a = 5.00 mm, b = 6.59 mm, d = 4.00 mm) and (a = 5.00 mm, b = 5.30 mm, d = 4.00 mm), respectively. Confirmation experiments show that the optimal results are reasonable with less than 4, 2, and 1% errors between the predicted and experimental data for the three mathematic models.

Finally, the developed optimization method based on PSO was used to optimize the floating cavity structure and layout of the heating rods for an actual industrial product of the LCD TV frame. The optimal design parameters for the layout of the heating

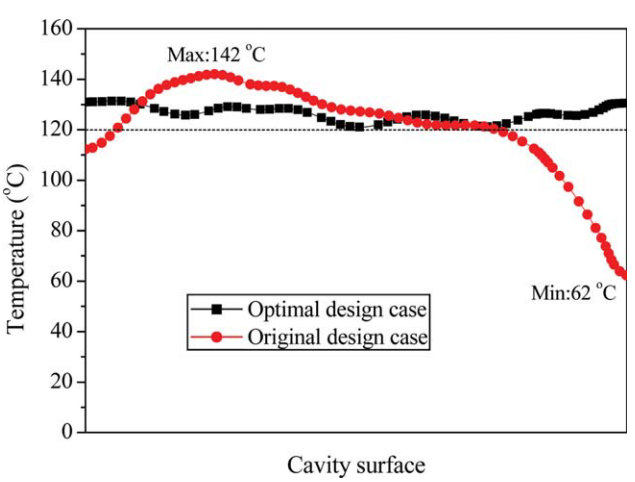

Figure 18 Temperature distribution on the cavity surface for the optimal and original design cases. [Color figure can be viewed in the online issue, which is available at wileyonlinelibrary.com.]

rods are $a = 5.00$ mm and $b = 6.45$ mm when the diameter of the heating rod is limited to be 6.00 mm. With the optimal results, an efficient design method based on part line, heating rod line, and cavity back surface line was proposed to design the structure of the floating cavity and identify the reasonable positions of the heating rods. The following heat transfer analysis results show that the optimal cavity structure has much more uniform temperature distribution than the original cavity structure. The maximum temperature difference of the cavity surface can be reduced from 80 to 10°C by utilizing the optimal design case. Additionally, the optimal deign case also has the potential to improve the service life of the floatable electric-heating cavity.

References

1. Wang, G. L.; Zhao, G. Q.; Li, H. P.; Guan, Y. J. Polym Plast Technol Eng 2009, 48, 671.
2. Zhao, G. Q.; Wang, G. L.; Guan, Y. J.; Li, H. P. Polym Adv Technol 2010 (to appear).
3. Lin, Y. W.; Li, H. M.; Chen, S. C.; Shen, C. Y. Int Commun Heat Mass Transfer 2005, 32(9), 1221.
4. Huang, M. S.; Tai, N. S. J Appl Polym Sci 2009, 113, 1345.
5. Yao, D. G.; Kimerling, T. E.; Kim, B. Polym Eng Sci 2006, 46, 938.
6. McCalla, B. A.; Allan, P. S.; Hornsby, P. R.; Smith, A. G.; Wrobel, L. Evaluation of pulsed cooling in injection mould tools. ANTEC Conf Proc 2004, 1, 461.
7. Chen, S. C.; Chang, Y.; Chang, T. H.; Chien, R. D. Int Commun Heat Mass Transfer 2008, 35, 130.
8. Chen, S. C.; Wang, Y. C.; Liu, S. C.; Cin, J. C. Sens Actuators A 2009, 151, 87.
9. Yao, D. G.; Kim, B. Polym Eng Sci 2002, 42, 2471.
10. Yao, D. G.; Kim, B. Appl Therm Eng 2003, 23, 341.
11. Xie, L.; Ziegmann, G. Microsystem Technol 2008, 14, 809.
12. Chen, S. C.; Jong, W. R.; Chang, J. A. J Appl Polym Sci 2005, 101, 1174.
13. Chen, S. C.; Lin, Y. W.; Chien, R. D.; Li, H. M. Adv Polym Technol 2008, 27, 224.
14. Chang, P. C.; Hwang, S. J. J Appl Polym Sci 2006, 102, 3704.
15. Yu, M. C.; Young, W. B.; Hsu, P. M. Mater Sci Eng A 2007, 460–461, 288.
16. http://www.gasinjection-ww.com/why-rtc.aspx, accessed 18 October 2009.
17. Wang, G. L.; Zhao, G. Q.; Li, H. P.; Guan, Y. J. Mater Des 2010, 31, 382.
18. Jansen, K. M. B. Heat transfer in injection moulding systems with insulation layers and heating elements. Int J Heat Mass Transfer 1995, 38, 309.
19. Yao, D. G.; Nagarajan, P.; Li, L.; Yi, A. Y. A strategy for rapid thermal cycling of molds in thermoplastic processing. J Manuf Sci Eng 2006, 128, 837.
20. Au, K. M.; Yu, K. M. Int J Adv Manuf Technol 2007, 34, 496.
21. Xu, R. X.; Sachs, E. Polym Eng Sci 2009, 49, 305.
22. Yao, D. G.; Chen, S. C.; Kim, B. Adv Polym Technol 2009, 27, 233.
23. Wang, G. L.; Zhao, G. Q.; Li, H. P.; Guan, Y. J. Mater Des 2010, 31, 3426.
24. Park, S. J.; Kwon, T. H. Polym Eng Sci 1998, 38, 1450.
25. Rao, N. S.; Schumacher, G.; Schott, N. R.; O'brien, K. T. J Reinforc Compos 2002, 21, 451.
26. Myers, R. H.; Montgomery, D. C. Response Surface Methodology, 2nd ed.; Wiley: New York, 2002.
27. Sachs, E.; Wylonis, E.; Allen, S. Polym Eng Sci 2000, 40, 1232.
28. Xu, X. R.; Sachs, E.; Allen, S. Polym Eng Sci 2001, 41, 1265.
29. Rannar, L. E.; Glad, A.; Gustafson, C. G. Rapid Prototyping J 2007, 13, 128.
30. http://www.matweb.com/, accessed 28 October 2009.
31. Cengel, Y. A.; Boles, M. A. In Thermodynamics: An Engineering Approach, 4th ed.; McGraw-Hill, New York, 2002.
32. Rao, Y. K. Tsay, K. J.; Wu, W. S.; Tzeng, Y. M. Process Biochem 2007, 42, 535.
33. Eberhart, R. C.; Kennedy, J. In Proceedings of Sixth International Symposium on Micro Machine and Human Science; IEEE Press: Nagoya, Japan, 1995; p 39.
34. Kennedy, J.; Eberhart, R. C. In Proceedings of IEEE International Conference on Neural Networks; IEEE Press: Perth, Australia, 1995; p 1942.
35. Suresh, S.; Sujit, P. B.; Rao, A. K. Particle swarm optimization approach for multi-objective composite box-beam design. Compos Struct 2007, 81, 598.
36. Chen, Y. Y.; Lin, J. T. Expet Syst Appl 2009, 36, 12264.
37. Chen, C. P.; Chuang, M. T.; Hsiao, Y. H.; Yang, Y. K.; Tsai, C. H. Expet Syst Appl 2009, 36, 10752.